Role of Interfacial and Intrinsic Coulomb Impurities in Monolayer MoS_2 FETs

Khadija A. Khair and Shaikh S. Ahmed
Department of Electrical and Computer Engineering
Southern Illinois University at Carbondale
Carbondale, Illinois 62901, USA
khadijakhair@siu.edu, ahmed@siu.edu

***Abstract*—In this work, first, 2D scattering rates in monolayer MoS_2 FETs due to interfacial and intrinsic Coulomb impurities as well as all other possible scatterers in an asymmetric dielectric environment have been calculated. Next, using the calculated 2D scattering rates, the electron mobility and current degradation in a monolayer MoS_2 based FET have been studied employing a particle-based quantum-corrected Monte Carlo device simulator. The intrinsic phonon-limited electron mobility is found to be around 10^5 $cm^2/V.s$. The interfacial effects (remote phonon and remote Coulomb scattering) degrade this value to ~36 $cm^2/V.s$ and intrinsic Coulomb scattering further reduces the electron mobility to ~3 $cm^2/V.s$. It is found that Coulomb scattering is responsible for ~92% of current degradation, while remote phonon and intrinsic phonon reduce the current by ~33% and ~10%, respectively. Among the Coulomb scattering rates, the remote Coulomb scattering from the top oxide (HfO_2) and the bottom oxide (SiO_2) reduce the current by ~24% and ~72%, respectively. Whereas, the intrinsic Coulomb scattering alone degrades the current by ~90%.**

Keywords—monolayer MoS_2, Coulomb scattering, phonon scattering, Monte Carlo device simulation

I. Introduction

While Silicon-based transistors approach their physical limit and naturally scaled-down 2D graphene layer has low ON/OFF current ratio, monolayer 2D molybdenum disulphide (MoS_2) holds promise as channel material for future field-effect transistors (FETs) with a finite non-zero energy bandgap and a high ON/OFF current ratio. Recently, a research team at the Lawrence Berkeley National Laboratory have demonstrated a 2-D MoS_2-CNT based transistor with a gate length of 1 *nm* [1]. MoS_2 transistors operating at gigahertz frequencies (with a cutoff frequency of ~6 *GHz*) have been reported in [2]. As for the electronic structure, in monolayer MoS_2, the *K*-point exhibits a direct bandgap of ~1.8 *eV*. The electron effective mass at the *K* point, $m_e^* = 0.48m_0$ and is isotropic [3]. Nevertheless, given the realistic construction of an FET with multiple contacts and interfaces, electron mobility in monolayer MoS_2 is degraded by various scattering mechanisms. In monolayer MoS_2, the 3-atom unit cell gives rise to 9 (nine) phonon branches (3 acoustic and 6 optical) [4]. Acoustic phonon-limited mobility has been calculated using Boltzmann equation and first-principles method [5] and found to be ~ 10^5 $cm^2/V.s$ at temperature, $T <$ 10 K and carrier density, $n \geq 10^{11}$ cm^{-2}. Whereas, room temperature phonon-limited mobility, considering both acoustic and optical modes, has been found to be ~410 $cm^2/V.s$ [6]. In [7], combined experimental and theoretical study on thinning induced mobility degradation in MoS_2 has been done. Here, the interfacial Coulomb impurities were identified as the dominant scatterers. Also, the role of individual scattering mechanisms in monolayer MoS_2 was evaluated by calculating electron mobility within an RTA (relaxation time approximation) framework. It was concluded that mobility in monolayer MoS_2 is mainly dominated by ionized impurity scattering [8]. However, this group calculated the scattering rates for *symmetric* dielectric environment and did not consider *remote* Coulomb scattering.

Recently, first-principles many-body calculations were done to obtain dielectric constant for monolayer MoS_2 [9]. For infinite layer separation, it was found that monolayer MoS_2 has a static dielectric constant of 1.0, whereas the previous studies reported the value in the range of 4.2-7.6. In this work, using this reported value of 1.0 for the static dielectric constant, we calculate the scattering rates in monolayer MoS_2 due to a) intrinsic phonon, b) remote phonon, c) intrinsic Coulomb and d) remote Coulomb processes. Since a realistic FET device has *asymmetric* dielectric environment, we did these calculations considering SiO_2 as the bottom oxide and HfO_2 as the top oxide. We then study the electron transport in a monolayer MoS_2 based FET device employing a particle-based Monte Carlo device simulator. Finally, the electron mobility and current degradation have been compared incrementally considering all possible scattering mechanisms.

II. Simulation Model

The simulations have been carried out using out in-house *Quantum Atomistic Device Simulator* (QuADS 3-D) [10][11]. QuADS 3-D, currently, enables quantum-corrected atomistic numerical modeling of non-equilibrium charge and phonon transport phenomena in realistically-sized systems containing more than 100 million atoms. In QuADS 3-D: a) material parameters are obtained atomistically using first-principles, b) structural relaxation and phonon dispersions are studied via molecular mechanics/dynamics, c) a variety of tight-binding models (*s, sp^3s^*, $sp^3d^5s^*$*) are used for the calculation of electronic bandstructure, and d) transport is simulated using a quantum-corrected Monte Carlo framework. The software tools used in QuADS 3-D exploit several recently developed

Supported by the U.S. National Science Foundation Grant No. 1610474.

978-1-5386-1016-9/18/$31.00 ©2018 IEEE

novel, memory-miserly, and fast algorithms, are portable, and incorporate state-of-the-art fault-tolerant software design approaches.

As for the Monte Carlo transport kernel, used in the current work, the following scattering mechanisms have been included: transverse acoustic (TA) phonon, longitudinal acoustic (LA) phonon, 0^{th}-order optical phonon, 1^{st}-order optical phonon, polar optical phonon, 0^{th}-order and 1^{st}-order surface/remote optical phonon from top gate oxide and buried oxide layers, remote Coulomb scattering in top gate oxide and buried oxide layers and intrinsic Coulomb scattering. Quantum mechanical size-quantization effects have been accounted for via a *parameter-free effective potential* scheme [12][13]. The approach is based on a perturbation theory around thermodynamic equilibrium and derived from the idea that the semiclassical Boltzmann equation with the quantum corrected potential and the Wigner equation should possess the same steady state. The effective potential possesses no fitting parameters, as the size of the electron (wavepacket) is determined from its energy. At present, impact ionization is not included in the model, as, for the drain biases used in the simulation, electron energy is typically in-sufficient to create electron-hole pairs. Also, band-to-band tunneling and generation and recombination mechanisms have not been included in the simulations.

A quasi-static assumption has been made for the holes. The Incomplete Lower-Upper (ILU) decomposition method has been employed for the solution of the 3-D Poisson equation. Also, in this kernel, to treat full Coulomb (electron-ion and electron-electron) interactions properly, the simulator implements two real-space *electron dynamics* (ED) schemes: the particle-particle-particle-mesh (P^3M) and the corrected Coulomb approach [14][15][16][17]. The effective force on an electron is computed as a combination of the short-range force and the long-range Poisson force. Also, necessary *event-biasing algorithms* are used in the simulator that enhance the carrier statistics and result in a faster convergence of the channel current [18].

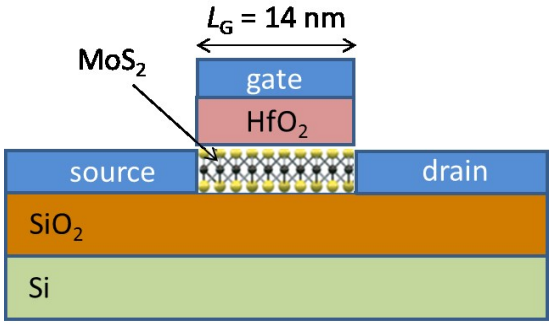

Fig. 1. Schematic of the simulated MoS_2 FET.

III. Results and Discussions

The simulated MoS_2 FET has a gate length of 14 *nm*, source-drain length of 15 *nm* and a device width of 50 *nm* (Fig. 1). The channel thickness is 0.65 *nm* (thickness of a single MoS_2 layer) and it is undoped. We have used HfO_2 as top gate oxide (with an equivalent oxide thickness, EOT, of 2 *nm*). The active MoS_2 channel sits on a SiO_2 buried oxide layer. In the beginning, the simulator was benchmarked against an experimental (longer) device reported in [2] for equilibrium condition giving rise to a sheet charge density of ~2×10^{12} cm^{-2} at a gate voltage, V_{GS} = 2 *V*. Also, for electron mobility, μ_n, of 200 $cm^2/V.s$, the calculated current was ~60 $\mu A/\mu m$, which is close to the experimentally measured value of ~50 $\mu A/\mu m$.

To capture the effect of dielectric mismatch between the semiconductor and its surrounding environment on the free-carrier screening of scattering potentials, Lindhhard function has been used in calculating the scattering rates [8]:

$$\varepsilon_{2D}(q,\omega\to 0)=1+\frac{e^2}{2\varepsilon_0\varepsilon_s q}\prod(q,T,E_F)(\Phi_1+\Phi_2), \qquad (1)$$

where, q is the 2D scattering wave vector, ε_S is the relative dielectric constant of semiconductor, Π is the static polarizability function for Fermi energy E_F and at finite temperature T, Φ_1 is the form factor and Φ_2 is the dielectric mismatch factor. In [8], the dielectric mismatch factor is defined for symmetric dielectric environment:

$$\Phi_2=\frac{2\chi_+\chi_-\exp(-qa)(\varepsilon_e-\varepsilon_s)^2-(\chi_-^2+\chi_+^2)(\varepsilon_e^2-\varepsilon_s^2)}{\exp(qa)(\varepsilon_e+\varepsilon_s)^2-\exp(-qa)(\varepsilon_e-\varepsilon_s)^2}, \qquad (2)$$

where, $\chi(y)=\sqrt{2/a}\cos(\pi y/a)$, $\chi_\pm=\int dy\exp(\pm qy)\chi^2(y)$, a is the thickness of the MoS_2 layer, and ε_e is the relative dielectric constant of surrounding environment. But, if the monolayer MoS_2 is surrounded by an asymmetric dielectric environment, which is the more realistic scenario for MoS_2 FETs, then the dielectric mismatch factor can be rewritten as in (3) shown at the bottom of the page: Here, ε_{ox} and ε_{box} are the relative dielectric constant of the top gate oxide and the bottom gate oxide respectively. Using this equation, we have recalculated all scattering mechanisms.

The Coulomb scattering rates have been determined using the following equation:

$$\frac{1}{\tau_{Coul}}=\frac{2D_0}{\hbar g_s g_v}\int_0^{\pi}\frac{|M_{kk'}|^2}{\varepsilon_{2D}^2}(1-\cos\theta)d\theta, \qquad (4)$$

where, D_0 is the 2D density-of-state and the matrix element for 2D Coulomb scattering is given as (see next page):

$$\Phi_2=\frac{2\chi_+\chi_-\exp(-2qa)\frac{\varepsilon_{ox}-\varepsilon_s}{\varepsilon_{ox}+\varepsilon_s}\frac{\varepsilon_{box}-\varepsilon_s}{\varepsilon_{box}+\varepsilon_s}-\chi_-^2\exp(-qa)\frac{\varepsilon_{ox}-\varepsilon_s}{\varepsilon_{ox}+\varepsilon_s}\chi_+^2\exp(-qa)\frac{\varepsilon_{box}-\varepsilon_s}{\varepsilon_{box}+\varepsilon_s}}{1-\exp(-2qa)\frac{\varepsilon_{ox}-\varepsilon_s}{\varepsilon_{ox}+\varepsilon_s}\frac{\varepsilon_{box}-\varepsilon_s}{\varepsilon_{box}+\varepsilon_s}} \qquad (3)$$

$$M_{kk'} = \frac{e^2}{2qS\varepsilon_0\varepsilon} \times 4 \left\{ \frac{\gamma}{\exp(qa) - \gamma} \frac{4\pi^2 \sinh\left(\frac{qa}{2}\right)}{4\pi^2 (qa) + (qa)^3} + \frac{2\left[1 - \exp\left(-\frac{qa}{2}\right)\right]\pi^2 + (qa)^2}{4\pi^2 (qa) + (qa)^3} \right\}, \quad (5)$$

where, S is the 2D surface area and $\gamma = \frac{\varepsilon_{ox} - \varepsilon_s}{\varepsilon_{ox} + \varepsilon_s} \frac{\varepsilon_{box} - \varepsilon_s}{\varepsilon_{box} + \varepsilon_s}$. For intrinsic Coulomb scattering, ε is the dielectric constant of the semiconductor (ε_s) and for remote/interfacial Coulomb scattering, $\varepsilon = (\varepsilon_s + \varepsilon_{ox})/2$, where ε_{ox} is the relative dielectric constant of the oxide associated with the interface. As we see in Fig. 2, intrinsic Coulomb scattering rate is very high as the relative dielectric constant of monolayer MoS_2 is too small ($\varepsilon_s \approx 1$). Also, the SiO_2 (bottom oxide) has a lower dielectric constant than that of HfO_2 (top oxide), therefore, the Coulomb potentials of the charged impurities are strongly suppressed at high-K dielectric/semiconductor interface.

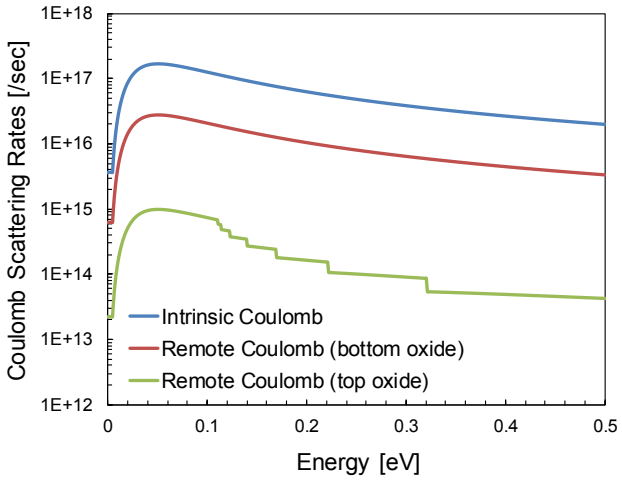

Fig. 2. The 2D Coulomb scattering rates for monolayer MoS_2.

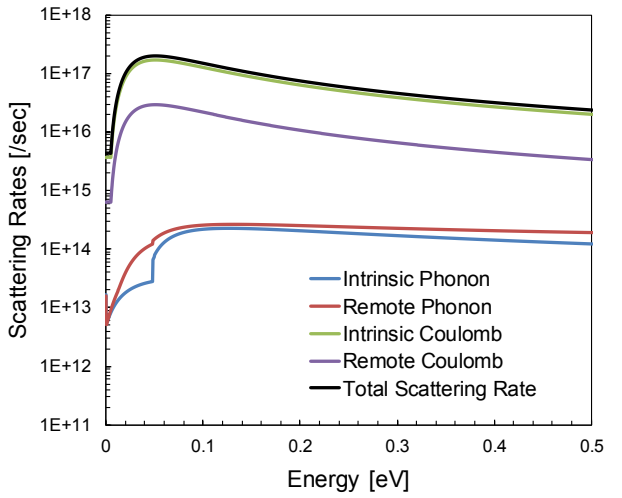

Fig. 3. The 2D scattering rates for monolayer MoS_2.

In Fig. 3, we plot all 2D scattering rates as well as the total scattering rate. As expected, the total scattering rate is dominated by intrinsic Coulomb scattering rate. Next two dominating scattering mechanisms are due to remote Coulomb and remote phonon processes. Overall, with an increase in electron energy, the total scattering rate first increases and then exhibits a gradual roll-off characteristic beyond 0.05 *eV*.

To further assess the impact of scattering processes, we calculate electron mobility in monolayer MoS_2 using the Rhode's iterative approach:

$$\mu = -\frac{1}{3} \frac{q\pi^2}{\sqrt{2m^*}} \frac{\int E\tau(E)v(E)\frac{\partial f}{\partial E}dE}{\int \sqrt{E} f(E) dE}, \quad (6)$$

where, E is the electron energy, $\tau(E)$ is the momentum relaxation time, $v(E)$ is the electron velocity and $f(E)$ is the distribution function. Electron concentration dependence of electron mobility is shown in Fig. 4. From the calculation, the room-temperature intrinsic phonon limited mobility is found to be as high as ~10^5 $cm^2/V.s$ for a carrier density of 5×10^{12} cm^{-2}. When interfacial effects are included (i.e. remote phonon and remote Coulomb scattering), the room-temperature mobility becomes as low as 36 $cm^2/V.s$. Electron mobility further degrades (down to ~3 $cm^2/V.s$) if any defects or impurities are present in the monolayer.

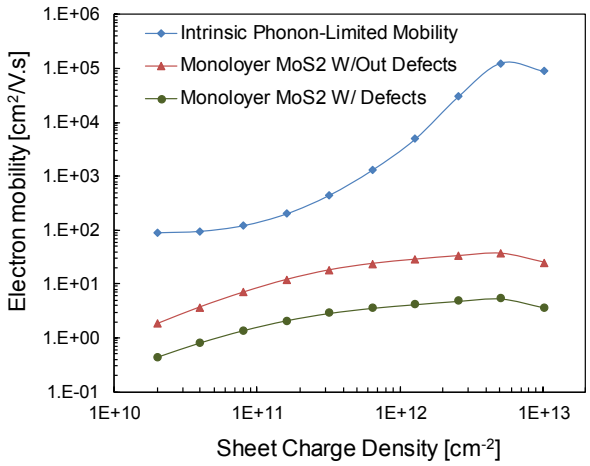

Fig. 4. Electron mobility in MoS_2 as function of sheet charge density, limited by different scattering processes.

Finally, using end-to-end particle-based Monte Carlo simulations, the degradation in the output drain current due to various scattering processes have been investigated and displayed in Fig. 5. With respect to a ballistic current of 161 $\mu A/\mu m$, it is found that Coulomb scattering is responsible for ~92% of current degradation, while remote phonon and intrinsic phonon reduce the current by ~33% and ~10%, respectively. Among the Coulomb scattering rates, the remote Coulomb scattering from the top oxide (HfO_2) and the bottom oxide (SiO_2) reduce the current by ~24% and ~72%, respectively. Whereas, the intrinsic Coulomb scattering alone degrades the current by ~90%.

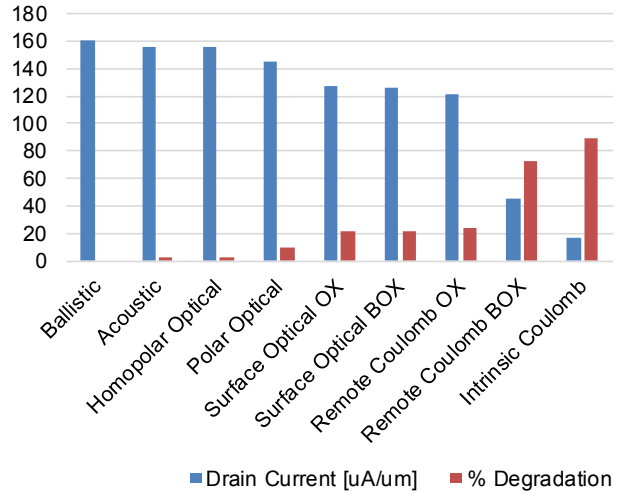

Fig. 5. Current and its degradation due to different scattering mechanisms.

IV. Conclusion

With a finite bandgap, single layer MoS_2 is preferable to graphene as a channel material. One of the main obstacles in MoS_2 is low electron mobility, which results in smaller ON current. The total scattering rate, which affects the electron mobility directly, is dominated by intrinsic Coulomb scattering process. For mechanically exfoliated monolayer MoS_2, which is cleaner than CVD-grown sheet, this type of scattering can be avoided and the total scattering rate can be reduced by 10 times. Next two dominating scattering mechanisms, namely, remote Coulomb and remote phonon scattering processes can be eliminated if suspended monolayer MoS_2 sheet can be used as the channel in the FET device. From our calculation, it is found that the room-temperature intrinsic phonon limited mobility can be as high as ~10^5 $cm^2/V.s$. *Intrinsic* Coulomb scattering degrades the mobility to as low as ~3 $cm^2/V.s$. If this process can be eliminated, the mobility increases to ~36 $cm^2/V.s$. Intrinsic Coulomb scattering is responsible for ~90% of current degradation as compared to the ballistic current. Whereas, the interfacial Coulomb scattering due to the SiO_2/MoS_2 interface and the HfO_2/MoS_2 interface degrades the drain current by ~72% and ~24%, respectively.

Acknowledgment

This work was supported by the U.S. National Science Foundation Grant No. 1610474.

References

[1] Sujay B. Desai, Surabhi R. Madhvapathy, Angada B. Sachid, Juan Pablo Llinas, Qingxiao Wang, Geun Ho Ahn, Gregory Pitner, Moon J. Kim, Jeffrey Bokor, Chenming Hu, H.-S. Philip Wong, Ali Javey, "MoS_2 transistors with 1-nanometer gate lengths," *Science*, vol. 354, no. 6308, pp. 99–102, 7 October 2016.

[2] D. Krasnozhon, D. Lembke, C. Nyffeler, Y. Leblebici, and A. Kis, "MoS_2 transistors operating at gigahertz frequencies," *Nano Lett.,* vol. 14, pp. 5905–5911, 2014.

[3] E. S. Kadantsev and P. Hawrylak, "Electronic structure of single MoS2 monolayer", *Solid State Commun*, vol. 152, no. 10, pp. 909–913, 2012.

[4] Y. Cai, J. Lan, G. Zhang and Y.-W. Zhang, "Lattice vibrational modes and phonon thermal conductivity of monolayer MoS_2," *Phys. Rev. B,* vol. 89, pp. 035438, 2014.

[5] K. Kaasbjerg, K. Thygesen and A.-P. Jauho, "Acoustic phonon limited mobility in two-dimensional semiconductors: Deformation potential and piezoelectric scattering in monolayer MoS_2 from first principle," *Phys. Rev. B*, vol. 87, pp. 235312, 2013.

[6] K. Kaasbjerg, K. Thygesen and K. Jacobsen, "First-principles study of the phonon-limited mobility in n-type single-layer MoS_2," *Phys. Rev. B,* vol. 85, pp. 115317, 2012.

[7] S.-L. Li, K. Wakabayashi, Y. Xu, S. Nakaharai, K. Komatsu, W.-W. Li, Y.-F. Lin, A. A.-Ferreira and K. Tsukagoshi, "Thickness-Dependent Interfacial Coulomb Scattering in Atomically Thin Field-Effect Transistors," *Nano Lett.*, vol. 13, pp. 3546-3552, 2013.

[8] F. Hüser, T. Olsen and K. S. Thygesen, "How dielectric screening in two-dimensional crystals affects the convergence of excited-state calculations: Monolayer MoS2," *Phys. Rev. B*, vol. 88, pp. 245309, 2013.

[9] F. Hüser, T. Olsen and K. S. Thygesen, "How dielectric screening in two-dimensional crystals affects the convergence of excited-state calculations: Monolayer MoS2," *Phys. Rev. B*, vol. 88, pp. 245309, 2013.

[10] S. Ahmed, K. Yalavarthi, V. Gaddipati, A. Muntahi, S. Sundaresan, S. Mohammed, S. Islam, R. Hindupur, D. John, and J. Ogden, "Quantum Atomistic Simulations of Nanoelectronic Devices using QuADS," in *Nano-Electronic Devices: Semiclassical and Quantum Transport Modeling*, book edited by D. Vasileska and S. M. Goodnick, Springer, pp. 405–441, 2011.

[11] S. Ahmed, M. Rashid, S. Al-Qahtani, Md R. K. Nishat, K. Khair, Y. Wu, A. Muntahi, M. Taher and A. Abdullah, "Multiscale and Multiphysics Modeling of Non-Classical Semiconductor Devices," ICECE 2016, *Proc. of 9th Int. Conference on Electrical and Computer Engineering*, Dhaka, Bangladesh, December 2016.

[12] S. Ahmed, C. Ringhofer, D. Vasileska, "Parameter-Free Effective Potential Method for Use in Particle-Based Device Simulations," *IEEE Trans. Nanotechnology*, vol. 4, pp. 465–471, July 2005.

[13] S. Ahmed, C. Ringhofer and D. Vasileska, ""Effective potential approach for modeling MOSFET devices," *Journal of Computational Electronics,* vol. 2, pp. 113–117, 2003.

[14] D. Vasileska and S. Ahmed, "Narrow-Width SOI Devices: The Role of Quantum Mechanical Size Quantization Effect and the Unintentional Doping on the Device Operation," *IEEE Trans. Electron Devices*, vol. 52, pp. 227–236, 2005.

[15] H. R. Khan, D. Vasileska, S. S. Ahmed, C. Ringhofer and C. Heitzinger, "Modeling of FinFET: 3D MC Simulation Using FMM and Unintentional Doping Effects on Device Operation," *J. Comput. Electron.,* vol. 3, pp. 337–340, 2004.

[16] D. Vasileska, H. R. Khan and S. S. Ahmed, "Modeling Coulomb Effects in Nanoscale Devices," *J. Comput. Theor. Nanosci.,* vol. 5, pp. 1793–1827, 2008.

[17] C. Heitzinger, C. Ringhofer, S. Ahmed and D. Vasileska, "3D Monte-Carlo device simulations using an effective quantum potential including electron-electron interactions," *J. Comput. Electron*., vol. 6, pp. 15, 2007.

[18] M. Nedjalkov, S. Ahmed, and D. Vasileska, "A self-consistent event biasing scheme for statistical enhancement," *Journal of Computational Electronics*, 3, pp. 305–309, 2004.